



## Validation of Aura Microwave Limb Sounder OH and HO<sub>2</sub> measurements

H. M. Pickett,<sup>1</sup> B. J. Drouin,<sup>1</sup> T. Canty,<sup>1</sup> R. J. Salawitch,<sup>1</sup> R. A. Fuller,<sup>1</sup> V. S. Perun,<sup>1</sup>  
 N. J. Livesey,<sup>1</sup> J. W. Waters,<sup>1</sup> R. A. Stachnik,<sup>1</sup> S. P. Sander,<sup>1</sup> W. A. Traub,<sup>1</sup>  
 K. W. Jucks,<sup>2</sup> and K. Minschwaner<sup>3</sup>

Received 10 April 2007; revised 28 September 2007; accepted 29 November 2007; published 24 May 2008.

[1] The Microwave Limb Sounder (MLS) instrument on the Aura satellite obtains global measurements of both OH and HO<sub>2</sub> radicals. This paper describes the precision and systematic errors of the MLS version v2.2 of the retrieval software. Estimated systematic errors are less than 8% for OH over 32–0.003 hPa and HO<sub>2</sub> over 6.8–0.21 hPa. Comparison of measurements from MLS OH and HO<sub>2</sub> profiles and three balloon-based instruments show good agreement among themselves and with a photochemical model using standard chemistry (i.e., recommended rate constants). Similarly, good agreement is seen between column OH found by integrating satellite profiles and ground-based measurements of column OH. The agreement between measured and modeled OH and HO<sub>2</sub> is improved following perturbations to the rate constants O + OH and OH + HO<sub>2</sub> that are within the recommended uncertainties. Measurements of OH obtained a decade ago by the Middle Atmosphere High-Resolution Spectrograph Investigation (MAHRSI) are smaller than MLS measurements by 20% at 70 km, are similar to MLS data near 50 km, and are 50% larger than MLS observations near 42 km. The MLS and MAHRSI measurements of OH overlap at the limit of their respective 2- $\sigma$  uncertainties. Most importantly, we find the shape of the OH profile measured by MLS is simulated well using standard chemistry.

**Citation:** Pickett, H. M., et al. (2008), Validation of Aura Microwave Limb Sounder OH and HO<sub>2</sub> measurements, *J. Geophys. Res.*, 113, D16S30, doi:10.1029/2007JD008775.

### 1. Introduction

[2] The Aura satellite was launched on 15 July 2004 into a sun-synchronous near-polar orbit. The Microwave Limb Sounder (MLS) instrument on the Aura satellite measures the hydroxyl radical (OH) and the peroxy radical (HO<sub>2</sub>) both day and night [Waters *et al.*, 2006]. Details on the THz module that measures OH and its calibration are given by Pickett [2006]. Details on the retrieval algorithms are given by Livesey *et al.* [2006]. Early validation of OH and HO<sub>2</sub> with balloon-borne remote sensing instruments is given in Pickett *et al.* [2006a]. Early validation of other molecules measured by MLS is given by Froidevaux *et al.* [2006]. The current version of the MLS retrieval software is v2.2 and is the current production software. All the data taken from launch to February 2007 has been processed with the earlier version v1.5. The data since launch will be reprocessed with version v2.2, but only selected days have been reprocessed

thus far. However, unless otherwise stated, this paper will use version v2.2. A description of the differences between these two major versions as it relates to HO<sub>x</sub> will be given below.

[3] Odd hydrogen (HO<sub>x</sub> = OH + HO<sub>2</sub> + H) chemistry dominates atmospheric ozone destruction at heights above 40 km [Osterman *et al.*, 1997] and below 22 km [Salawitch *et al.*, 2005]. Observations of OH over 40–80 km from the Middle Atmosphere High-Resolution Spectrograph Investigation (MAHRSI) [Conway *et al.*, 2000] were not consistent with standard chemistry (JPL recommended rates). Photochemical models could not reconcile with MAHRSI data over 40–80 km using adjusted rate constants for known reactions. Changes needed to fix the mesospheric OH made the situation worse at 40 km, leading to the designation “HO<sub>x</sub> dilemma.” However, balloon-borne observations that are mostly sensitive to HO<sub>x</sub> below 40 km agree better with photochemical theory [Jucks *et al.*, 1998] and with MLS measurements of HO<sub>x</sub> [Canty *et al.*, 2006].

### 2. MLS Measurements

#### 2.1. Overview

[4] The Aura satellite was launched on 15 July 2004 into a sun synchronous orbit with a 1375 LST ascending node equatorial crossing. The Microwave Limb Sounder is one of four instruments included on the satellite. For latitudes near

<sup>1</sup>Jet Propulsion Laboratory, California Institute of Technology, Pasadena, California, USA.

<sup>2</sup>Harvard-Smithsonian Center for Astrophysics, Cambridge, Massachusetts, USA.

<sup>3</sup>New Mexico Institute of Mining and Technology, Socorro, New Mexico, USA.

**Table 1.** Target Molecule Line-Center Frequencies for MLS HO<sub>x</sub> Bands

| Band   | Molecule        | Frequency, GHz |
|--------|-----------------|----------------|
| 15, 18 | OH              | 2514.317       |
| 16, 19 | OH              | 2509.949       |
| 16, 19 | O <sub>3</sub>  | 2509.560       |
| 17, 20 | O <sub>2</sub>  | 2502.324       |
| 17, 20 | O <sub>3</sub>  | 2543.208       |
| 28     | HO <sub>2</sub> | 649.702        |
| 30     | HO <sub>2</sub> | 660.486        |

34°N, the MLS overpass occurs at 1330 local solar time (LST) and again at 0230 LST. At latitudes above 70° up to the orbital inclination limit of 83°, the MLS overpass LST changes rapidly. MLS scans vertically in the plane of the orbit. Consequently, the longitude of the MLS footprint changes by 24° each orbit. For consistency with other measurements on MLS, retrieved profiles are archived in volume mixing ratio units on pressure surfaces with 6/decade vertical resolution.

[5] The OH measurements are made with a THz receiver [Pickett, 2006] that uses a gas laser as the local oscillator [Mueller et al., 2007]. There are six receiver bands (15–20) in the THz receiver, each connected to a 25-channel filter bank. The filters near the center of each band are 6 MHz wide, and the width increases to 96 MHz at  $\pm 575$  MHz from band center. Four of these bands (15,16,18,19) are used to observe OH. In addition there are two receiver bands (17,20) that are used for pointing information. The frequencies of the target lines are shown in Table 1 and an example of the observed radiance is shown in Figure 1.

[6] The OH lines indicated in Table 1 are each split into 3 hyperfine components [Blake et al., 1986]. There are two THz mixers, one for each of two different linear polarizations, that provide simultaneous measurements to improve the OH signal to noise ratio. Bands 15–17 and bands 18–20 have perpendicular polarizations, with axes that are oriented  $\sim 26^\circ$  from nadir. The Zeeman splitting is  $\sim \pm 1$  MHz and, in the small splitting limit, the polarization differences can be shown to be proportional to the square of the ratio of the Zeeman shift to the Doppler width (6 MHz). Therefore, measurements from the two polarizations are fitted simultaneously by a model of unpolarized emission. Bands 16 and 19 have an O<sub>3</sub> line at the edge from which an O<sub>3</sub> profile is retrieved. While the noise associated with the THz O<sub>3</sub> profile is large compared with the O<sub>3</sub> profile from the GHz bands, comparison of the THz profile with GHz O<sub>3</sub> gives added information on systematic errors.

[7] The THz module retrieves pointing information from bands 17 and 20 using a magnetic dipole line of O<sub>2</sub> in the lower sideband and a strong line of O<sub>3</sub> in the upper sideband. Band 20 does not have a dedicated filter bank, but the filter bank used nominally for 640-GHz N<sub>2</sub>O can be switched to band 20. During instrument check out shortly after launch, the band 20 performance was measured and bore-sight offsets were determined. Since then the instrument has been configured for N<sub>2</sub>O measurements and band 20 data is not available. An example of the observed band 17 radiance is shown in Figure 2.

[8] The HO<sub>2</sub> measurements are made from two HO<sub>2</sub> lines in the 640 GHz radiometer each using a 11-channel mid-

band filter bank. These filter banks are identical in design to the center channels of the standard 25-channel filter bank and are embedded in the frequency space of other bands. Data from all the filter banks in the 640 GHz radiometer are used to retrieve profiles for eight other molecules in addition to HO<sub>2</sub>. An example of the observed radiance is shown in Figure 3. The HO<sub>2</sub> signal is only  $\sim 1$  K and signal/noise is  $\sim 3$  after a zonal average over 120° latitude. Consequently, 12 d of data are needed to obtain a zonal mean over a 10° latitude range with the same signal/noise as shown in Figure 3.

[9] A day-night HO<sub>2</sub> difference is required to reduce systematic errors to an acceptable level. The actual radiances in band 28 and 30 corresponding to the differences shown in Figure 3 are quite large due in part to absorption

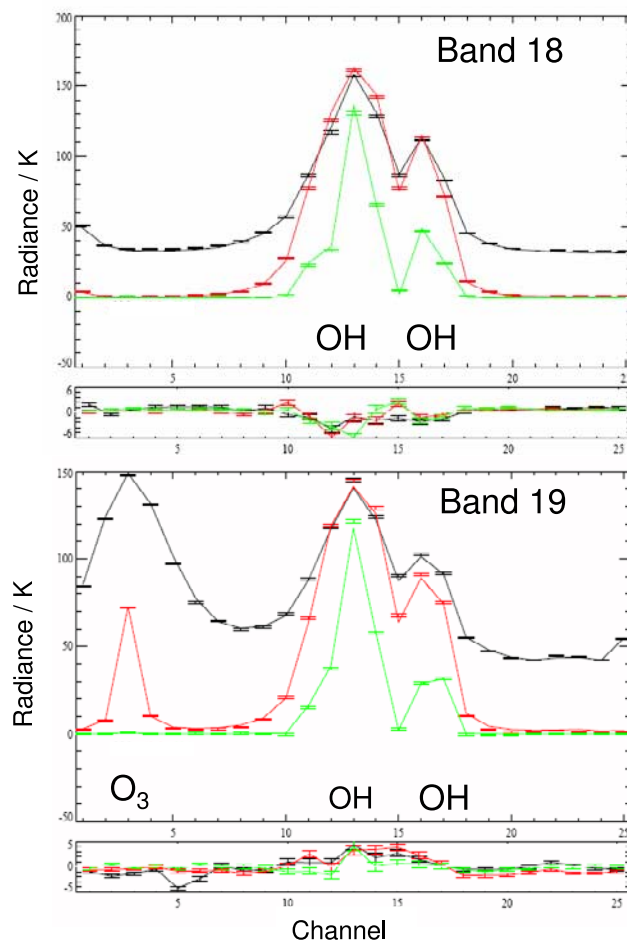


**Figure 1.** MLS radiance and residuals for bands 18 and 19. The OH emission shown here is composed of three hyperfine components. Radiance is a daylight zonal average over latitudes from 60°S to 60°N for 28 January 2005. The radiance is nearly identical for bands 15 and 16. The horizontal axis is the filter bank channel number. The vertical axis is radiance in K. The black, red, and green plots are for tangent heights of 31.5, 40.7, and 62.5 km, respectively. The solid lines in the large panels are the predicted radiance, and the center point of the error bars indicate the observed radiance. The small panels show the residuals for the observed minus calculated radiance.

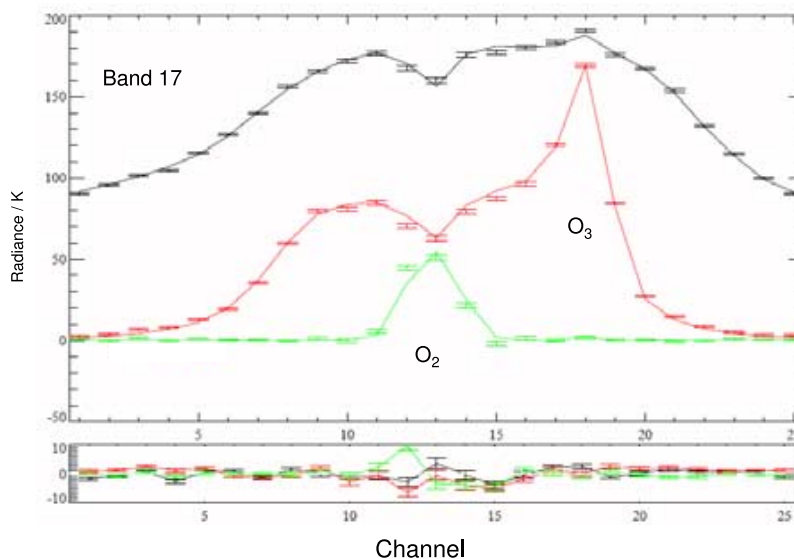


**Figure 2.** MLS radiance and residuals for band 17. The O<sub>2</sub> emission is in the lower sideband, and the THz O<sub>3</sub> emission is in the upper sideband. This band provides pointing information. Radiance shown here is a daylight zonal average over latitudes from 60°S to 60°N on 28 January 2005. See Figure 1 for further details.

by ozone. In band 28 at 40 km tangent height the background radiance is 25 K, while for band 30 the radiance changes from 50 K to 100 K across the band. The day-night differencing works for pressures above 0.03 hPa. Below this pressure there can be significant HO<sub>2</sub> at night due to the long reactive lifetimes of HO<sub>x</sub> at these low pressures [Pickett *et al.*, 2006b], but use of data below this pressure is also not recommended because of undue influence of a priori profiles.

[10] The MLS Level 2 data (retrieved geophysical parameters and diagnostics at the measurement locations along the suborbital track) are generated from input Level 1 data (calibrated radiances and engineering information) by the MLS data processing software. The MLS retrieval algorithms, described in detail by Livesey *et al.* [2006], are based on the standard optimal estimation method. They employ a two-dimensional approach that takes into account the fact that limb observations from consecutive scans cover significantly overlapping regions of the atmosphere. The results are reported in Level 2 Geophysical Product (L2GP) files, which are standard HDF-EOS version 5 files containing swaths in the Aura-wide standard format [Livesey *et al.*, 2006] (available from the MLS web site, <http://mls.jpl.nasa.gov>). A separate L2GP file is produced for each standard MLS product for each day (0000–2400 UT).

## 2.2. Data Screening

[11] Examples of the THz spectra and residuals for daytime are shown in Figures 1 and 2. To obtain radiance closure such as that shown in Figures 1 and 2, it is essential to screen the data using 3 pieces of information from the L2GP swath structure:

[12] 1. Use only even values of STATUS. Profiles with odd STATUS are flagged by the level 2 retrieval software for various errors that are described by other bits in the STATUS word (see Table 2).

[13] 2. Use only positive precision values. The precision field is flagged by the level 2 software with a negative sign when the estimated precision is 50% of the a priori precision. Negative precisions usually appear at the edge of the useful pressure range.

[14] 3. Use only scans with CONVERGENCE < 1.1. This field contains additional information on the success of the retrieval and compares the fit profiles to that expected by the linearized retrieval, with values around 1.0 typically indicating good convergence. A cutoff of 1.1 is a compromise between eliminating pathological nonconverging fits and keeping fits that have adequately converged.

[15] For some seasons, the Gas Laser Local Oscillator (GLLO) for the THz receiver is automatically relocked as many as 5 times during a day. These relock events occur when the tuning range of the laser is less than the thermal excursion over an orbit and over a day. This thermal effect depends on the albedo of the Earth as seen by the GLLO radiator. In these cases the status flag is 257 and the profile is ignored. This is only a problem for mapping because the missing data may appear at the same latitude and longitude on successive days.

[16] Over the pressure range of 32–10 hPa, one should use day-night differences to reduce biases. The recommended range for OH is 32–0.003 hPa.

[17] An example of the spectra and residuals in the 640 GHz radiometer near the two HO<sub>2</sub> lines are shown in Figure 3. The radiance shown is a day-night difference. The data filtering procedure is identical to that for the THz OH retrievals. Recommended range for HO<sub>2</sub> is 21–0.03 hPa.

## 2.3. Resolution and Precision

[18] The resolution of the retrieved profiles is described by the averaging kernels. Because the level 2 processing uses a two-dimensional retrieval, the averaging kernel has both a vertical component and a horizontal component in

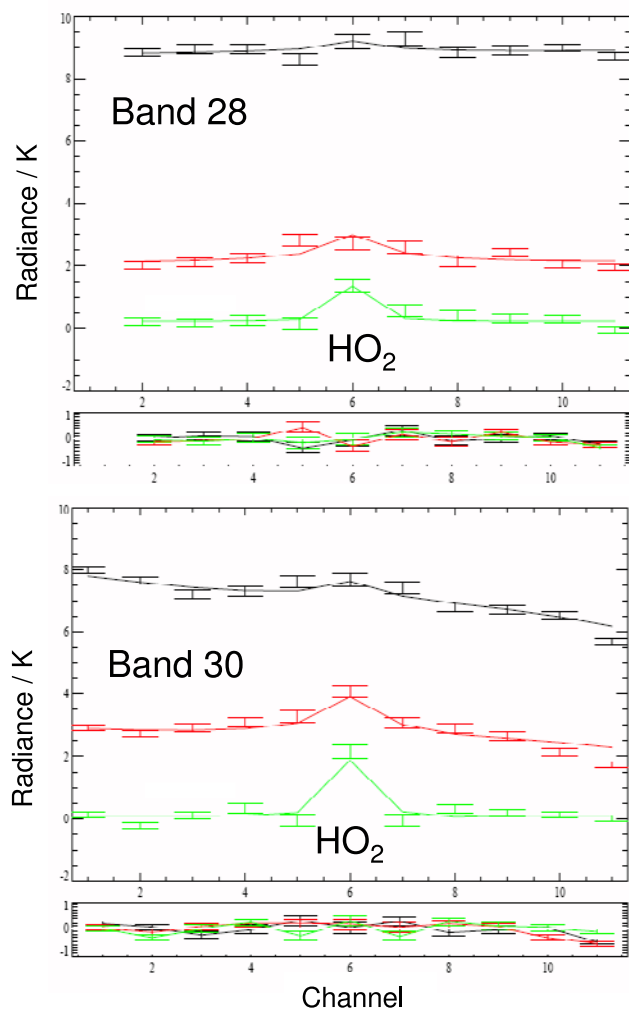


**Figure 3.** MLS radiance and residuals for bands 28 and 30. The radiance shown is a day-night difference of zonal averages for latitudes from 60°S to 60°N on 28 January 2005. See Figure 1 for further details.

the direction of the line of sight. Perpendicular to the line of sight the spatial resolution is determined by the horizontal width of the antenna pattern and is 1.5 km (HO<sub>2</sub>) to 2.5 km (OH).

[19] Figure 4 shows typical two-dimensional (vertical and horizontal along-track) averaging kernels for the MLS v2.2 OH data at 70°N. Variation in the averaging kernels is sufficiently small that these are representative for all profiles. Colored lines show the averaging kernels as a function of MLS retrieval level, indicating the region of the atmosphere from which information is contributing to the measurements on the individual retrieval surfaces, which are denoted by plus signs in corresponding colors. The dashed black line indicates the resolution, determined from the full width at half maximum (FWHM) of the averaging kernels, approximately scaled into kilometers (top axis). Figure 4 (top) shows vertical averaging kernels (integrated in the horizontal dimension for 5 along-track scans) along with the resolution (dashed line). The solid black line shows the integrated area under each kernel (horizontally

and vertically). Values near unity imply that the majority of information for that MLS data point has come from the measurements, whereas lower values imply substantial contributions from a priori information. Figure 4 (bottom) shows horizontal averaging kernels (integrated in the vertical dimension) along with the resolution (dashed line). The averaging kernels are scaled such that a unit change is equivalent to one decade in pressure. The vertical width of the averaging kernel at pressures above 0.01 hPa is 2.5 km. The horizontal width of the averaging kernel is equivalent to a width of 1.5° (165 km) distance along the orbit and is equivalent to one scan interval (24.67 s). The changes in vertical resolution below pressures below 0.01 hPa are due mainly to use of a faster operational scan rate for tangent heights above 70 km.

[20] Figure 5 shows typical two-dimensional (vertical and horizontal along-track) averaging kernels for the MLS v2.2 HO<sub>2</sub> data at 70°N. Details about Figure 5 and associated averaging kernel are the same as OH given above. The vertical width of the averaging kernel at pressures above 0.1 hPa is 4 km. The horizontal width of the averaging kernel is 2–4 profiles or a 3–6° distance along the orbit. In software version v2.2, smoothing of the profile was applied to reduce indeterminacy in the fit that was manifested in v1.5 as a vertical oscillation in the profile. The effect of the smoothing in v2.2 is to broaden the vertical averaging kernels to a width of 4 km and to broaden the horizontal averaging kernel by a factor of 2–4.

[21] A typical OH concentration profile and associated precision estimate is shown in Figure 6. The profile is shown both in volume mixing ratio (vmr) and density units. All MLS data are reported in vmr for consistency with the other retrieved molecular profiles. However, use of density units (10<sup>6</sup> cm<sup>-3</sup>) reduces the apparent steep vertical gradient of HO<sub>x</sub> allowing one to see the profile with more detail. Additionally, at THz frequencies the collisional line width is approximately equal to the Doppler width at 1 hPa. At pressures below 1 hPa Doppler broadening is dominant and the peak intensity of OH spectral absorption is proportional to density. At pressures above 1 hPa, the peak intensity is proportional to vmr. The daytime OH density profile shows

**Table 2.** Meaning of Bits in the “Status” Field

| Bit | Value <sup>a</sup> | Meaning   |
|-----|--------------------|---|
| 0   | 1                  | flag: do not use this profile<br>(see bits 8–9 for details)   |
| 1   | 2                  | flag: this profile is “suspect”<br>(see bits 4–6 for details)                                       |
| 2   | 4                  | unused  |
| 3   | 8                  | unused  |
| 4   | 16                 | information: this profile may have<br>been affected by high-altitude clouds                         |
| 5   | 32                 | information: this profile may have<br>been affected by low-altitude clouds                          |
| 6   | 64                 | information: this profile did not use<br>GEOS-5 temperature a priori data                           |
| 7   | 128                | unused  |
| 8   | 256                | information: retrieval diverged or too<br>few radiances available for retrieval                     |
| 9   | 512                | information: the task retrieving data<br>for this profile crashed<br>(typically a computer failure) |

<sup>a</sup>“Status” field in L2GP file is total of appropriate entries in this column.



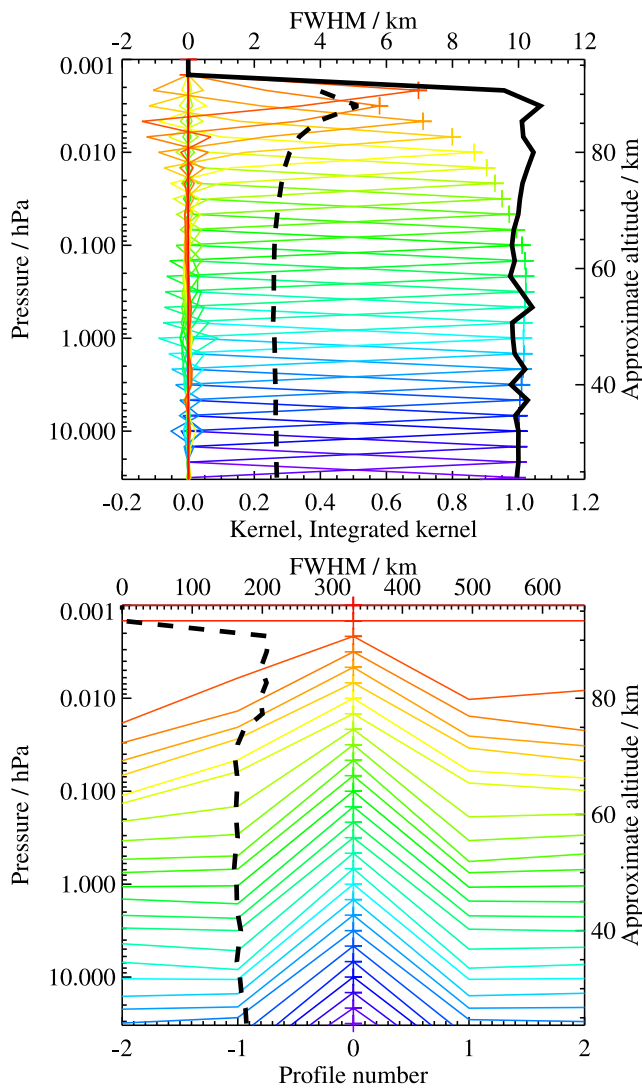


**Figure 4.** Typical two-dimensional (vertical and horizontal along-track) averaging kernels for the MLS v2.2 OH data at 70°N. (top) Vertical averaging kernels for OH. (bottom) The horizontal averaging kernels along the line of sight. The individual colored plots are the averaging kernels. The dashed black line is the width of the kernel (top axes), and the solid black line is its integral (bottom axes).

two peaks at  $\sim 45$  km and  $\sim 75$  km that are not as apparent in the vmr-based profiles. The night profile of OH exhibits the narrow layer at  $\sim 82$  km that has been described earlier [Pickett *et al.*, 2006b]. Precisions are such that an OH zonal average with a  $10^\circ$  latitude bin can be determined with better than 10% relative precision with 1 d of data (100 samples) over 21–0.01 hPa. With 4 d of data, the 10% precision limits can be extended to 32–0.0046 hPa.

[22] A typical HO<sub>2</sub> concentration profile and associated precision estimate is shown in Figure 7. The profile is shown both in volume mixing ratio (vmr) and density units. Precisions are such that a HO<sub>2</sub> zonal average with a  $10^\circ$  latitude bin can be determined with better than 10%

relative precision from 20 d of data (2000 samples) over 21–0.032 hPa.

#### 2.4. Expected Accuracy and Error Characterization

[23] A major component of the validation of MLS data is the quantification of the various sources of systematic uncertainty. Systematic uncertainties arise from instrumental issues: e.g., radiometric calibration, field of view characterization, spectroscopic uncertainty, and approximations in the retrieval formulation and implementation. This section summarizes the relevant results of a comprehensive quantification of these uncertainties that was performed for all MLS products. More information on this assessment is given by Read *et al.* [2007, Appendix A].

[24] The impact on MLS measurements of radiance (or pointing where appropriate) of each identified source of systematic uncertainty has been quantified and modeled. These modeled impacts correspond to either  $2\text{-}\sigma$  estimates of uncertainties in the relevant parameters, or an estimate of their maximum reasonable errors based on instrument knowledge and/or design requirements. The effect of these

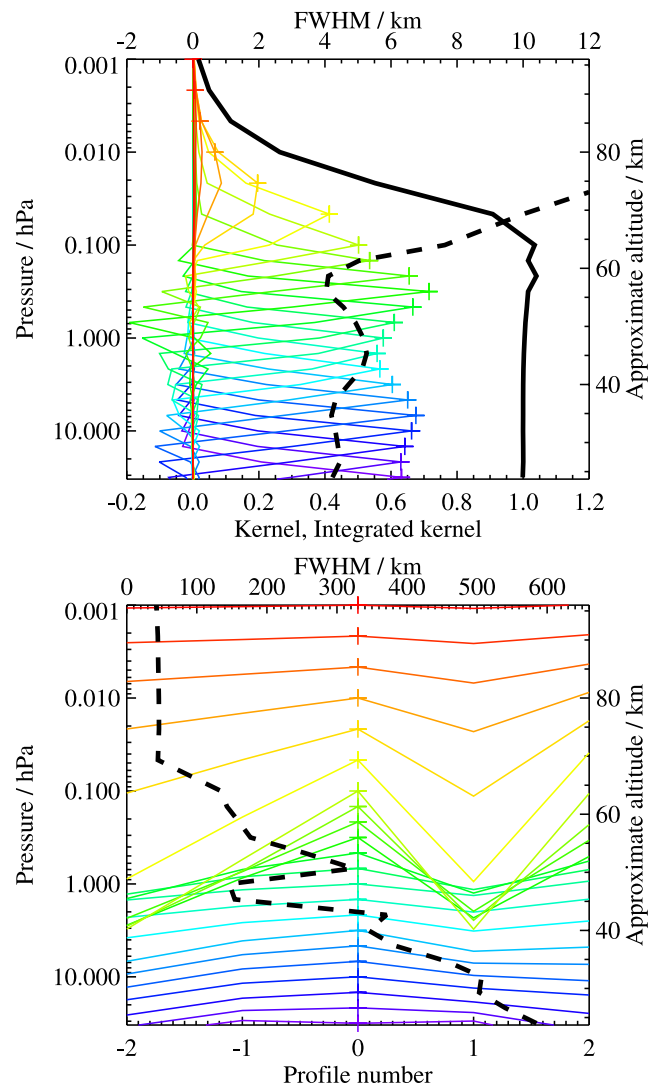


**Figure 5.** Averaging kernels for HO<sub>2</sub>. See Figure 4 for further details.

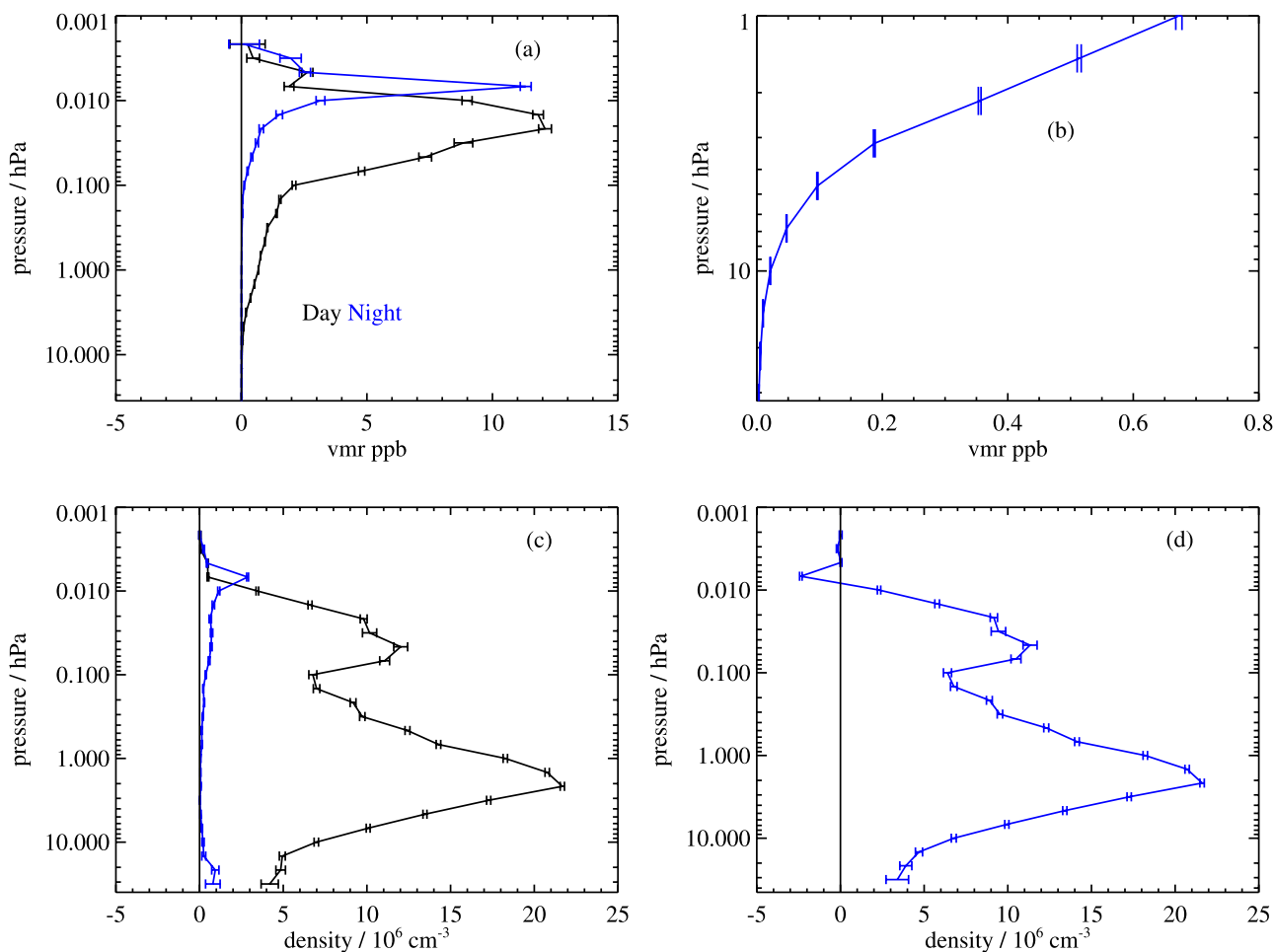


**Figure 6.** Zonal mean of retrieved OH and its estimated precision (horizontal error bars) for 20 September 2005 averaged over 29°N to 39°N. The average includes 368 profiles. (a) Plot of vmr versus pressure for day (black) and night (blue) overpasses. (b) The same data plotted for the stratosphere. (c) The same data converted to density units. (d) The day-night differences for the data in Figure 6c.

perturbations on retrieved MLS products has been quantified for each source of uncertainty by one of two methods.

[25] In the first method, sets of modeled errors corresponding to the possible magnitude of each uncertainty have been applied to simulated MLS cloud-free radiances, based on a model atmosphere, for a whole day of MLS observations. These sets of perturbed radiances have then been run through the routine MLS data processing algorithms, and the differences between these runs and the results of the “unperturbed” run have been used to quantify the systematic uncertainty in each case. The impact of the perturbations varies from product to product and among uncertainty sources. Although the term “systematic uncertainty” is often associated with consistent additive and/or multiplicative biases, many sources of “systematic” uncertainty in the MLS measurement system give rise to additional scatter in the products. For example, although an error in the O<sub>3</sub> spectroscopy is a bias on the fundamental parameter, it has an effect on the retrievals of species with weaker signals (e.g., HNO<sub>3</sub> that is dependent on the amount and morphology of atmospheric ozone). The extent to which such terms can be expected to average down is estimated to first order by these “full up studies” through

their separate consideration of the bias and scatter each source of uncertainty introduces into the data. The difference between the retrieved product in the unperturbed run and the original “truth” model atmosphere is taken as a measure of uncertainties due to retrieval formulation and numerics.

[26] In the second method, the potential impact of some remaining (typically small) systematic uncertainties has been quantified through calculations based on simplified models of the MLS measurement system [see *Read et al.*, 2007]. Unlike the “full up studies,” these calculations only provide estimates of “gain uncertainty” (i.e., possible multiplicative error) introduced by the source in question. This approach does not quantify possible biases or additional scatter for these minor sources of uncertainty.

[27] Finally, although the MLS observations are unaffected by thin cirrus clouds or stratospheric aerosols, thick clouds associated with deep convection can have an impact on the MLS radiances. The MLS Level 2 data processing algorithms discard or downplay radiances identified (through comparison with predictions from a clear-sky model) as being strongly affected by clouds [*Livesey et al.*, 2006]. The contribution of cloud effects to the systematic

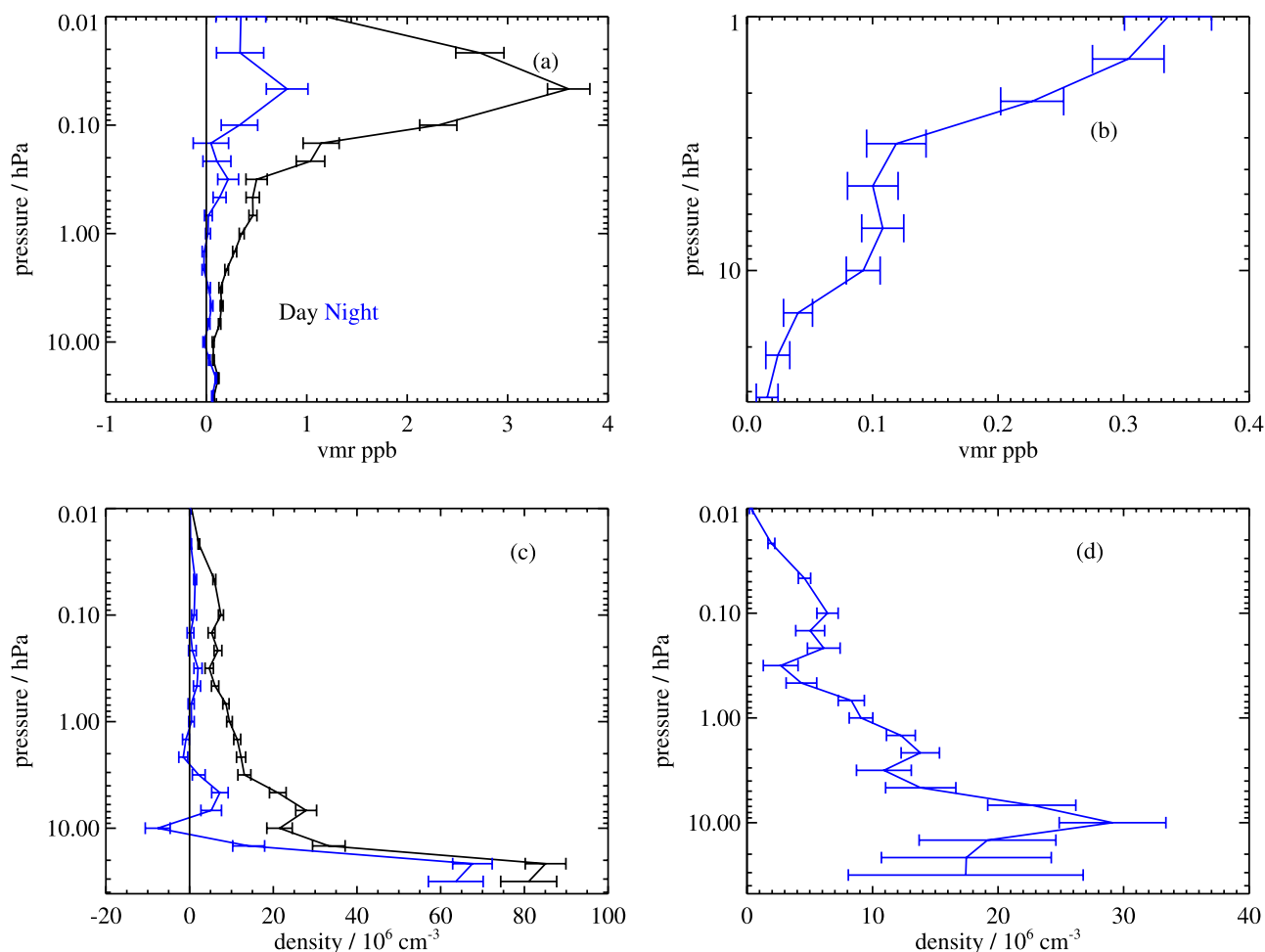


**Figure 7.** Zonal mean of retrieved HO<sub>2</sub> and its estimated precision for 20 September 2005 averaged over 29°N to 39°N. The average includes 2879 profiles. (a) Plot of vmr versus pressure for day (black) and night (blue) overpasses. (b) The same data plotted as a day-night difference for the stratosphere. (c) The same data converted to density units. (d) The day-night differences for the data in Figure 7c.

uncertainty, both from the presence of clouds not thick enough to be screened out by the cloud filtering and from the loss of information through omission of cloud-impacted radiances, has been quantified by adding scattering from a representative cloud field to the simulated radiances and comparing retrievals based on these radiances to the unperturbed results. The cloud-induced effects shown in Figures 8 and 9 are estimated by considering only the cloudy profiles (as defined by the known amount of cloud in the “truth” field). The contribution of clouds to HO<sub>x</sub> systematic errors is negligible in part because the high pressure limit of 31–22 hPa is much lower than the pressures expected for thick clouds. The thin polar mesospheric clouds are also not observable at MLS wavelengths.

[28] The estimated impacts of the systematic errors on OH are summarized in Figure 8. The largest contributors to systematic bias errors contributing to the systematic bias errors is the radiometric and spectral calibration category. The two biggest contributors to this category are sideband fraction and gain compression and are approximately equal. The multiplicative errors are estimated to be less than 8% for pressures above 0.02 hPa. The dominant contributor to the slope error below 0.02 hPa is sideband fraction. The size

of the OH errors relative to a typical profile can be seen by using a profile such as that in Figure 6.

[29] An independent measure of the effect of sideband fraction uncertainty is to compare O<sub>3</sub> retrieved from the THz radiometer with that retrieved from the GHz radiometers. A comparison given by *Froidevaux et al.* [2008] shows that the ratio of the O<sub>3</sub> concentrations is unity within 5% over 1–32 hPa. The uncertainty in OH due to sideband fraction should be the same as the uncertainty in the O<sub>3</sub>(THz)/O<sub>3</sub>(GHz) ratio. A complicating factor is that O<sub>3</sub>(THz) line in bands 16 and 19 has a much stronger temperature dependence than O<sub>3</sub>(GHz) lines. The calculated ratio of absorption coefficients changes by 1.7%/K, so the effect of temperature on the ozone ratio is small but not negligible. We therefore extend the low-pressure boundary of the region with systematic errors that are <8% to 0.03 hPa.

[30] An independent view of the effect of a priori assumptions can be determined by synthetic calculations of radiance. It is important to have several measures of the contribution of a priori assumptions to the data. Figure 10 shows an example of such a calculation. Here the night a priori profile contributes 7% to the output data at

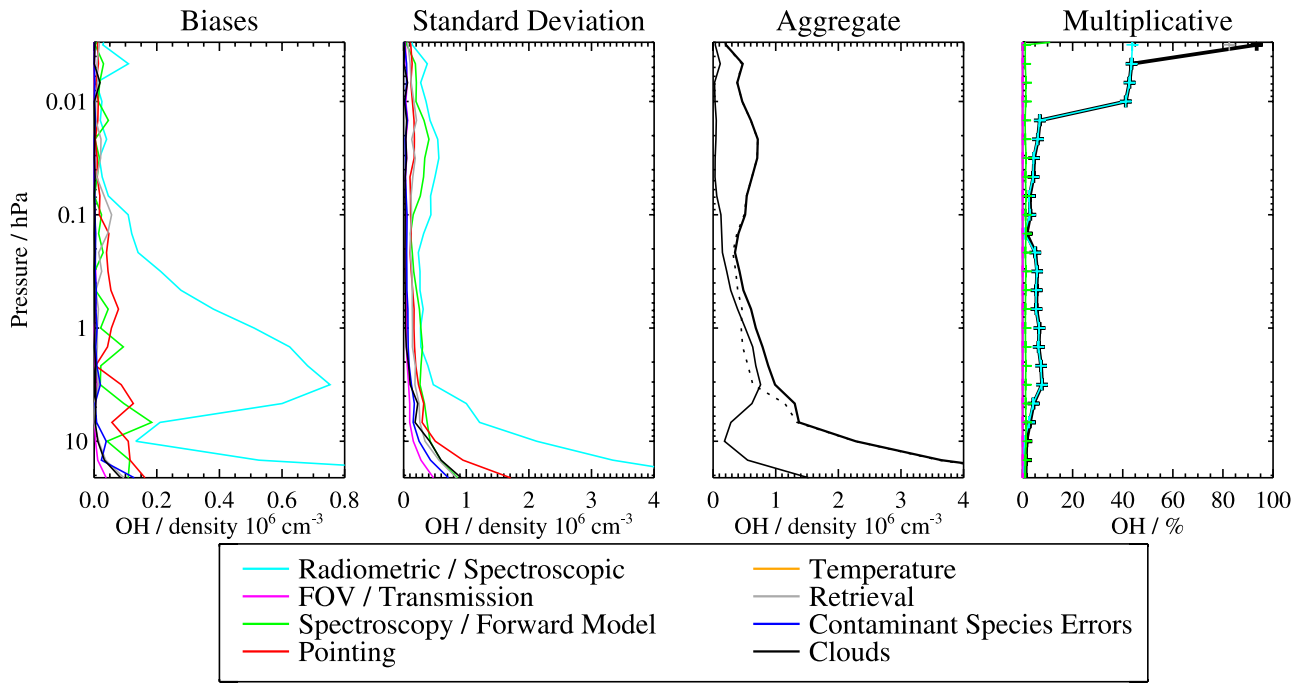


**Figure 8.** The estimated impact of various families of systematic errors on the MLS OH observations using day-night differences. The first two panels show the possible biases that are independent of concentration (first panel) and additional scatter introduced by the various families of errors (second panel), with each family denoted by a different colored line. The third panel shows the root sum squares (RSS) of all the possible biases (thin solid line), all the additional scatters (thin dotted line), and the RSS sum of the two (thick solid line). The fourth panel shows errors that are proportional to the concentration.

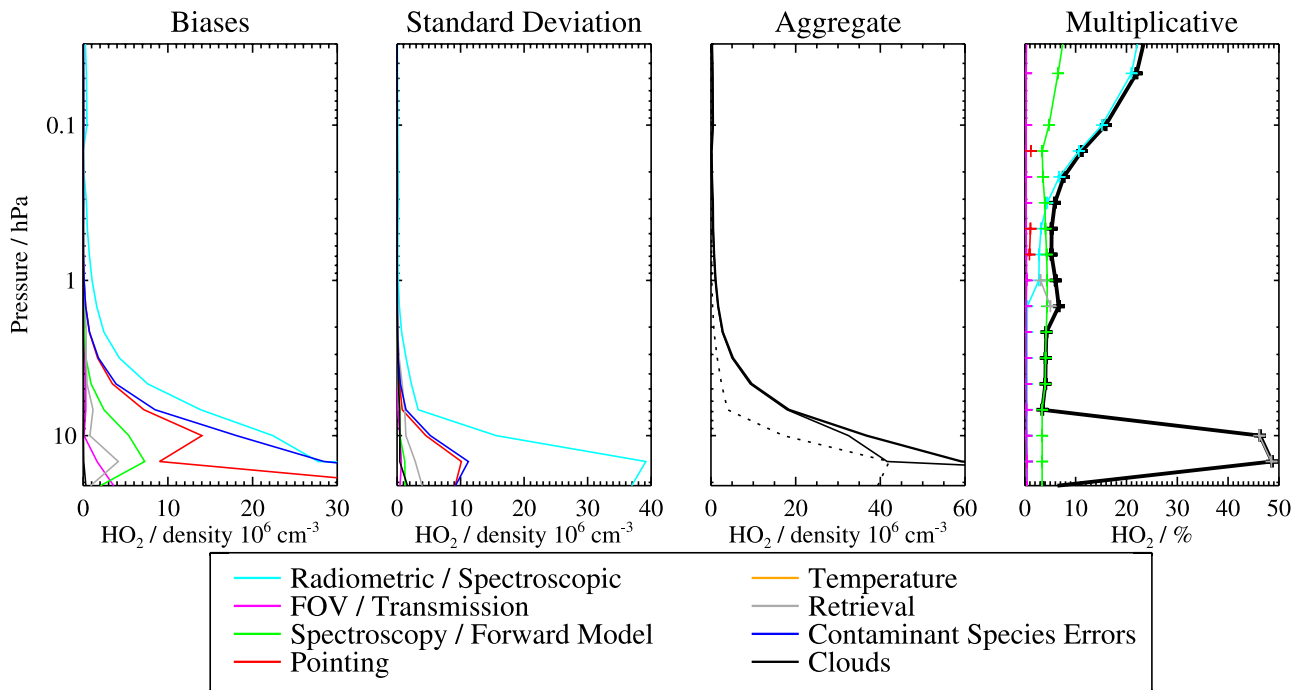


**Figure 9.** The estimated impact of various families of systematic errors on the MLS HO<sub>2</sub> observations of day-night differences. The first two panels show the possible biases (first panel) and additional scatter introduced by the various families of errors (second panel), with each family denoted by a different colored line. For further details, see Figure 8.



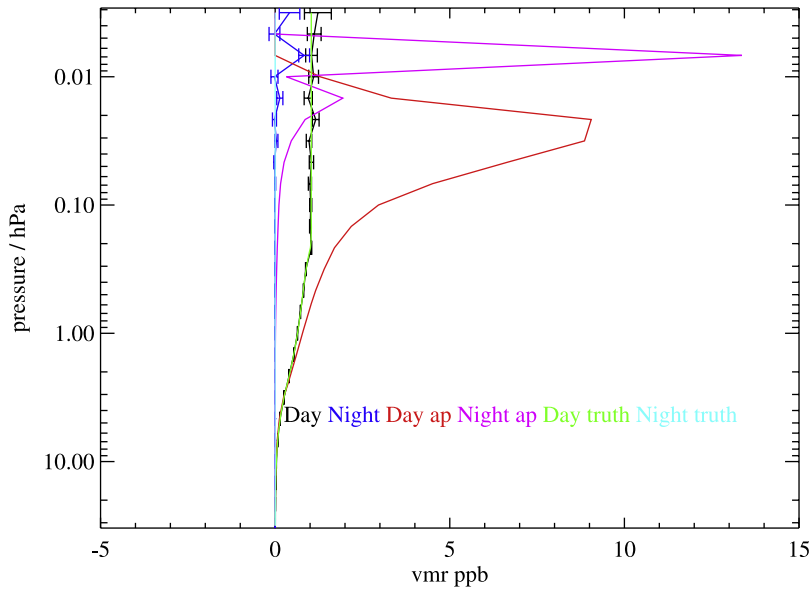


**Figure 10.** Retrieval results for synthetic OH profiles. The green line is the profile used to generate the synthetic daytime radiances. The red line is the daytime a priori profile. The black line with error bars is the retrieval output for the daytime profile and overlaps the green line. The error bars are the precision based on an estimated radiance uncertainty. No noise was added to the radiance. The night input profile (blue) was zero. The magenta line that peaks at 0.007 hPa is the night a priori profile. The blue line with error bars is the output retrieval for night.

0.0068 hPa. The large daytime peak in the a priori at 0.03 hPa shows no impact on differences between the assumed profile and the retrieved profile and the amount of a priori mixing is even smaller than at higher altitudes.

[31] The systematic errors on HO<sub>2</sub> retrieved concentration are summarized in Figure 9. The largest contributor of bias errors are sideband fraction and gain compression within the

category of radiometric and spectral calibration. Again, the systematic errors from sideband fraction and gain compression are approximately equal. Both contribute to the low altitude peak in bias and standard deviation. The slope error has a peak at 10 hPa due to a priori and radiometric numerics [Read *et al.*, 2007]. The slope error <0.1 hPa is due to filter position uncertainty. The size of the HO<sub>2</sub>

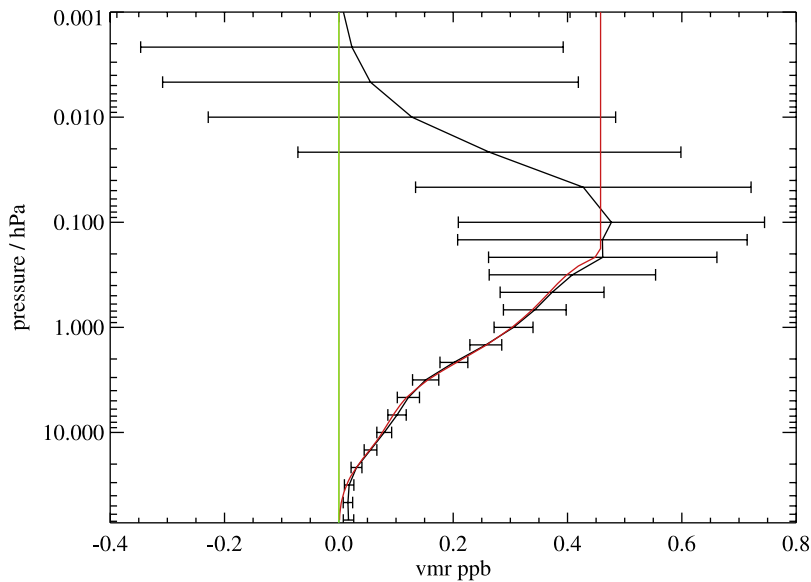


**Figure 11.** Retrieval results for synthetic HO<sub>2</sub> profiles. The red line is the profile used to generate the synthetic radiances. The black line is the retrieval output. The green line at zero is the a priori profile. The error bars are the precision based on a theoretical estimated radiance uncertainty. No noise was added to the radiance.

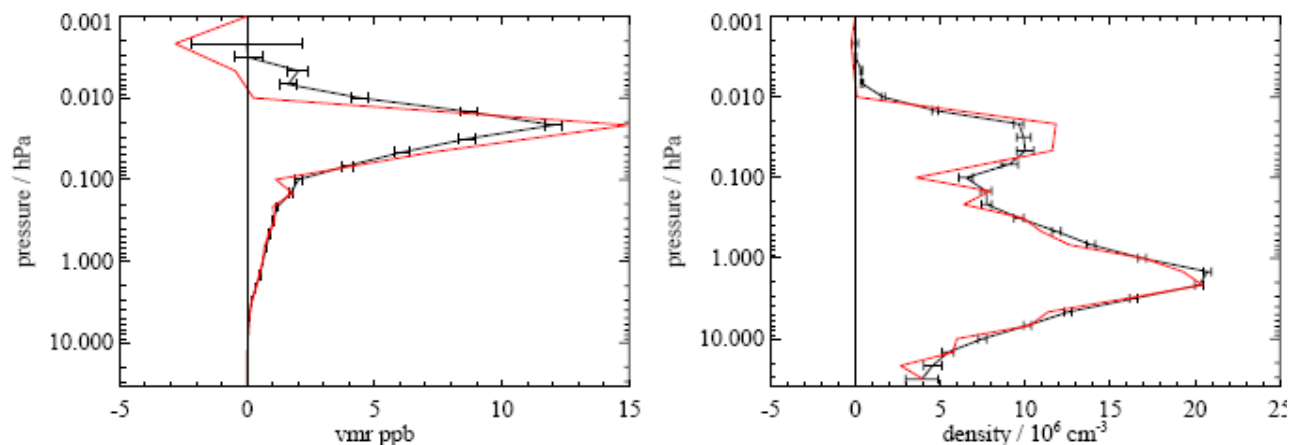


**Figure 12.** Comparison between v1.5 and v2.2 for MLS OH for 23 September 2004 zonally averaged over 29–39°N latitude. Red is version v1.5 and black is version v2.2. The same data is plotted in (left) vmr and (right) density.

systematic errors relative to a typical profile can be seen using Figure 7.

[32] The effect of a priori assumptions can also have an important effect on the HO<sub>2</sub> data. Figure 11 shows a retrieval that uses synthetic radiance derived from an input profile that is constant above 0.1 hPa. The a priori concentration profile is zero throughout. The retrieval tracks the input profile below 0.1 hPa. For pressures below 0.032 hPa there is at least 20% a priori contamination.

## 2.5. Differences Between Software Versions v2.2 and v1.5

[33] For the THz radiometer data in v2.2, the first step for level 1 calibration of MLS emission is to calibrate the data using a procedure that is a slight modification from the calibration described by Pickett [2006] for v1.5. The need for calibration change was found by examining the on-orbit variation of gain as a function of orbital phase. The gain has an approximately sinusoidal dependence on orbital phase that is 2 to 4% of the average value with a magnitude that depends on the filter channel. The gain change is needed to account for small thermal effects on gain over the orbit. In v1.5, the gain was assumed to be constant over the orbit. In v2.2, the fitted gain is now assumed to have an additional sinusoidal dependence on orbital phase as well as the constant dependence assumed in v1.5.1. The second change in v2.2 calibration is that the radiometric zero is derived only from the space view, whereas before in v1.5 it was derived from both the space view and the calibration target. This change makes small radiances less sensitive to assumptions about the gain. Both changes are part of v2.2 level 1 processing. The result is that the OH radiance has better calibration, improving accuracy by as much as 2%.

[34] In the OH v1.5 retrieval, the profiles were fitted to a pressure level interval of 3/decade below 0.1 hPa and 6/decade at higher pressures. In v2.2 the profile sampling is 6/decade over the whole pressure range. There are many beneficial changes in OH above 50 km as can be seen in Figure 12. The profiles are smoother, have uniform pressure resolution, and have much fewer instances of negative concentration. In the stratosphere, OH fits are less subject

to convergence problems in part because the iteration limit has been increased from 4 to 6.

[35] The main change for HO<sub>2</sub> is that there is more smoothing applied in version 2.2. In v1.5, no effective smoothing was applied and the profiles tended to have a small but significant oscillation in concentration with height. This kind of behavior is often an indication that the retrieval fitting is almost indeterminant, and the smoothing in v2.2 is effective in reducing this problem. The effect of smoothing at altitudes below 60 km is to broaden the averaging kernel to 4 km FWHM in the vertical and as much as 6 degrees along the track. Because of smoothing, precisions are no longer flagged negative above 60 km (0.1 hPa). However, it is estimated that there is at least 20% a priori contamination for pressures below 0.032 hPa (see above).

[36] The second change for v2.2 was to set the HO<sub>2</sub> a priori concentration to zero. The v1.5 HO<sub>2</sub> a priori concentrations were based on the results of model calculations. This change was made to avoid potential artifacts in smoothing due to the a priori assumptions. With zero a priori HO<sub>2</sub> and finite a priori uncertainty, the effect of a priori assumptions will be to lower the retrieved HO<sub>2</sub> relative to truth.

## 3. Comparisons With Other Data Sources

### 3.1. Comparison With Balloon-Borne Instruments

[37] Aura MLS validation campaigns took place in September 2004, 2005 involving balloon-borne instruments flown from Fort Sumner, NM (latitude = 34.5° and longitude = -104°). The Balloon OH instrument (BOH) and the Far Infrared Spectrometer (FIRS-2) instrument were launched on a common balloon gondola on 23 September 2004. Details of the 2004 flight are given by Pickett *et al.* [2006a]. During the 2005 flight, the Submillimeter Limb Sounder (SLS) accompanied the BOH and FIRS-2 instruments. The balloon stayed aloft at ~38 km for nearly 24 h for this flight. The results of all these measurements are summarized in Figure 13 along with a calculated profile from a photochemical model.

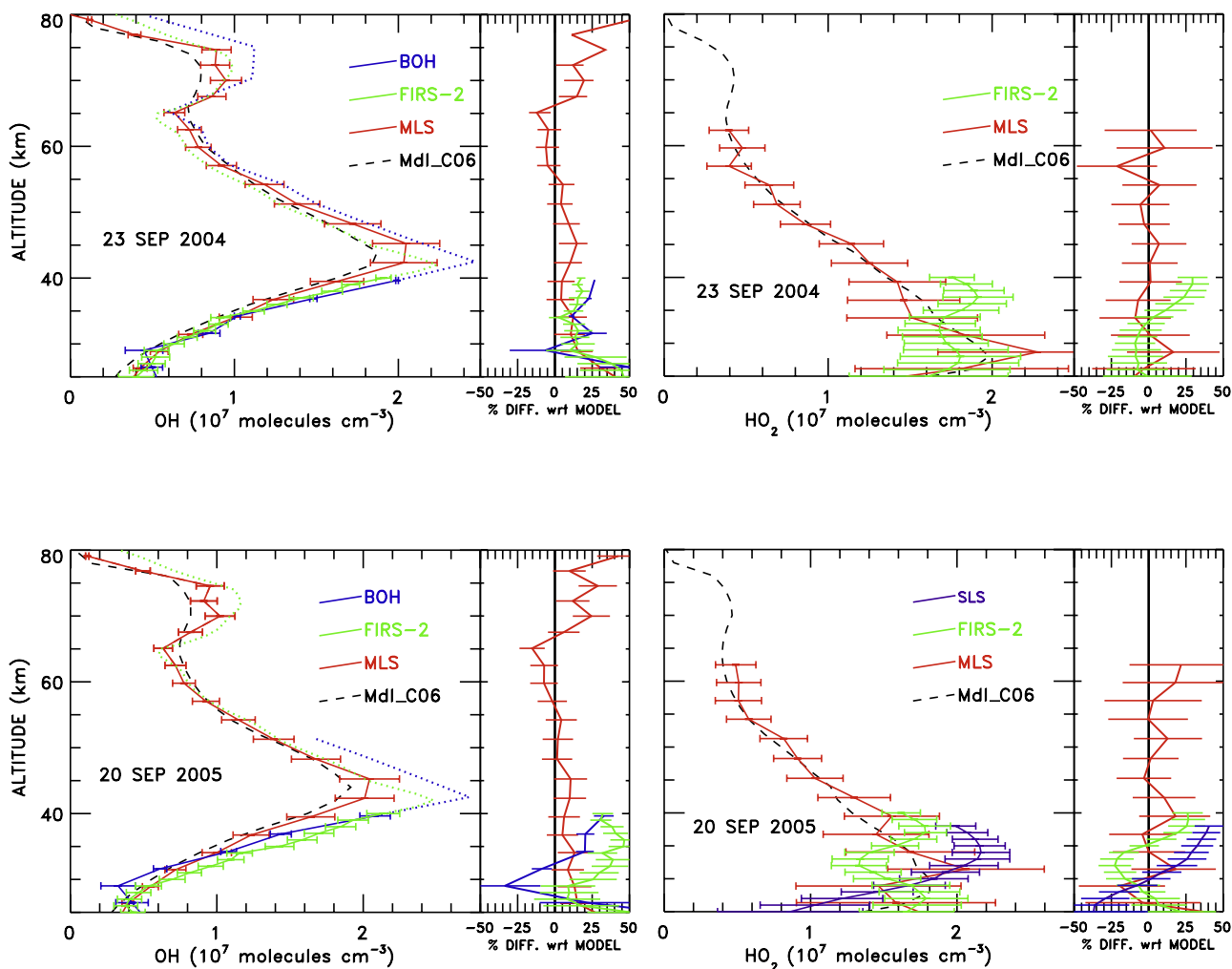


**Figure 13.** Balloon-borne HO<sub>x</sub> observations for 23 September 2004 and 20 September 2005 near Fort Sumner, NM, USA. (top) Using a zonal mean of MLS OH over a latitude range of 29–30°. (bottom) Using a 9-d zonal mean of MLS HO<sub>2</sub> over the same latitude interval. The balloon-borne instrument profiles above 40 km are shown as dotted lines to indicate the assumed profile. The balloon data and model calculations are for the time of the MLS overpass.

[38] The MLS OH profiles are a zonal mean over 29–39°N latitude. The MLS HO<sub>2</sub> profiles for 2004 are a zonal mean over latitudes <50°. The mean solar zenith angle (42°) was close to the solar zenith angle at the time of the closest overpass (39°). The MLS HO<sub>2</sub> profiles for 2005 are a zonal mean over 24–44°N latitude for 9 d centered on the day of the balloon flight.

[39] The BOH instrument is a heterodyne limb-viewing thermal emission instrument that is functionally identical to the THz module on MLS [Pickett *et al.*, 2006a] and only measures OH. The FIRS-2 instrument is a thermal emission far-infrared Fourier transform spectrometer developed at the Smithsonian Astrophysical Observatory [Jucks *et al.*, 1998]. It measures OH and HO<sub>2</sub> in the far infrared using multiple lines. SLS [Stachnik *et al.*, 1992] is a cryogenic heterodyne instrument that measures atmospheric radiance in the same spectral region as the MLS 640 GHz region. One of the molecules measured by SLS is HO<sub>2</sub>. The balloon instruments all use limb sounding to increase the effective path length. However, there is only an increase for tangent

heights below the balloon altitude. The path lengths for layers above the balloon are an order of magnitude smaller than at the tangent height. Accordingly, the balloon instruments have only 1–2 independent pieces of information above the balloon. The dotted lines for the profiles in Figure 13 show the assumed OH distribution that was used for each of the balloon retrievals. In all cases, the error bars are 1- $\sigma$  total error (precision and accuracy).

[40] Pickett *et al.* [2006a] reported good agreement (within 17% over 25–40 km) between the 2004 balloon and satellite observations of OH from 25–40 km. Observations of HO<sub>2</sub> agreed within 23% below 40 km.

[41] Here, the September 2004 comparisons have been updated using the v2.2 MLS retrievals and a current version of the photochemical model, Mdl\_C06 (see below), that incorporates JPL 2006 kinetics [Sander *et al.*, 2006]. Furthermore, this analysis has been extended to the 2005 observations. Figure 13 (top left) compares the new MLS OH retrieval for 2004 to the FIRS-2 and BOH measurements. Compared to the previously published comparisons,

there is better agreement (within 15%) between balloon observations of OH and the new MLS retrievals. The oscillations in the MLS HO<sub>2</sub> profile reported by *Pickett et al.* [2006a] are notably absent in the updated version (Figure 13, top right). Also, the error bars shown reflect the formulation for instrument precision described above. The agreement between HO<sub>2</sub> observations has improved to within 18%.

[42] The HO<sub>2</sub> measurements overlap with the two balloon measurements within a combined experimental error of 20%. The precision for day-night differences has been multiplied by  $3^{1/2}$  to account for the effects of the width of the horizontal averaging kernel (3 scans). There is no evidence that multiplicative systematic errors are as large as is shown in Figure 9. However, significant differences in HO<sub>2</sub> exist among the three instruments (Figure 13, bottom right). From 30 to 35 km the FIRS-2 and SLS instruments disagree by as much as 34%. The reason for this discrepancy is unclear at this time.

[43] The same comparisons for the 2004 validation campaign are carried out for the September 2005 flights. The agreement among OH observations is  $\pm 18\%$  (Figure 13, bottom left). However, the peaks in OH inferred from the OH partial column above float measured by FIRS-2 ( $2.5 \times 10^7$  molecules cm<sup>-3</sup>) and BOH ( $2.7 \times 10^7$  molecules cm<sup>-3</sup>) are larger than the peak observed by MLS ( $2.0 \times 10^7$  molecules cm<sup>-3</sup>) and outside of the MLS error bars. The MLS HO<sub>2</sub> measurements overlap with the two balloon measurements within a combined experimental error of 20%. However, there are significant differences between FIRS-2 and SLS from 30 to 35 km which need further study. There is no evidence that multiplicative systematic errors are as large as is shown in Figure 9. Figure 13 shows that MLS and the model agree within the MLS precision.

[44] The study by *Canty et al.* [2006] compared model results that tested combinations of kinetics parameters to the observations from 2004. They determined that best agreement was found between the MLS observations of OH, HO<sub>2</sub>, OH/HO<sub>2</sub>, and HO<sub>x</sub> and a model using JPL 2002 kinetics [*Sander et al.*, 2003], the rate for O + OH suggested by *Smith and Stewart* [1994], and a 20% increase in OH + HO<sub>2</sub> (denoted Mdl\_C or Mdl\_C02). These changes in the two rates are within their assigned uncertainty, but give improvements in the agreement between the model and earlier MLS results. Mdl\_C06 uses the same modification of the two reaction rates without further adjustment, but incorporates JPL 2006 kinetics [*Sander et al.*, 2006]. The model is constrained to MLS observations of H<sub>2</sub>O, O<sub>3</sub>, N<sub>2</sub>O, CO, and temperature appropriate to the dates of each validation campaign. Methane and nitric acid are inferred from N<sub>2</sub>O through tracer relationships. The reduced chi square ( $\chi_r^2$ ) values between MLS observations and model for 2004 and 2005 are shown in Figure 14. A  $\chi_r^2$  value of unity or less indicate model results within the experimental error. Results for both years are presented for MLS v1.5 and Mdl\_C02 (black bars) and MLS v2.2 and Mdl\_C06 (blue bars). There is overall improved agreement between model and observations for both days, primarily due to updated HO<sub>2</sub> retrievals, which are averaged more than the previous version, and the better formulation for the precision associated with these observations. It should be emphasized that the two rate constant adjustments were not reoptimized

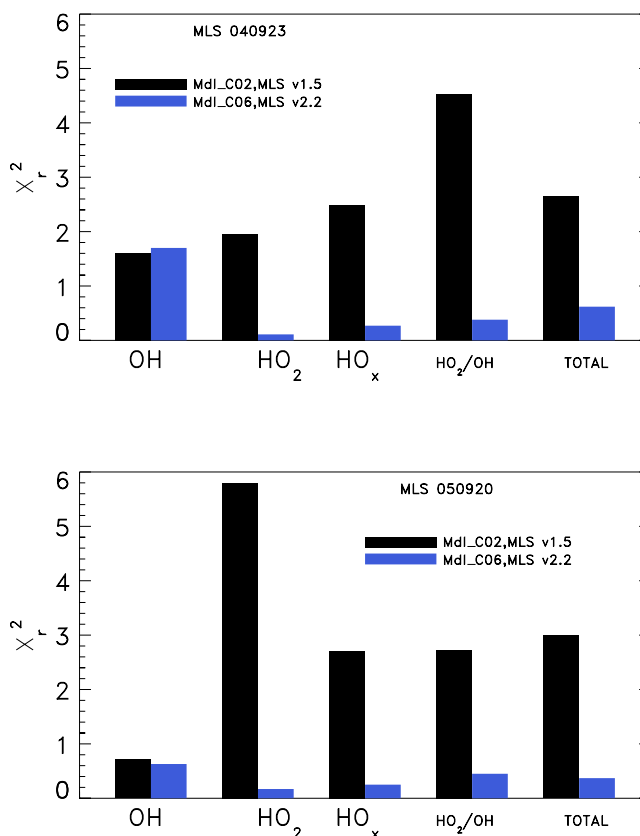


**Figure 14.** Comparison between model and MLS OH and HO<sub>2</sub> for 23 September 2004 and 20 September 2005. Black bars are v1.5 retrievals and blue bars are v2.2.

between Mdl\_C02 and Mdl\_C06. In addition, MLS v1.51 was used by *Canty et al.* [2006] and MLS v2.2 is used here.

### 3.2. Comparison With Ground-Based Column Measurements

[45] At the time of the 23 September 2004 balloon flight, both the Poly-Etalon Pressure Scanned Interferometric Optical Spectrometer (PEPSIOS) instrument [*Minschwaner et al.*, 2003] and the Fourier Transform Ultraviolet Spectrometer (FTUVS) instrument [*Cageao et al.*, 2001] were observing the OH column in absorption against the Sun at 308 nm. The PEPSIOS instrument was located in Socorro, New Mexico, USA (34°N, 107°W) and the FTUVS was located at Table Mountain, California, USA (34.5°N, 117.7°W). The observations are shown in Figure 15. The model in the dashed line is Mdl\_C06 described above. The solid line is JPL06 rate constants [*Sander et al.*, 2006] with no modification. BOH, FIRS-2, and MLS were corrected by adding both a tropospheric column using data of *Wennberg et al.* [1998] and an additional contribution from the boundary layer [*Singh et al.*, 2006]. The contribution from both these two sources of tropospheric OH is 7% of the total column. Both sources make similar contributions to the column. See Appendix A for further details.

[46] As before, the agreement between different column measurements is within most error estimates. PEPSIOS observations are generally higher than the FTUVS observations, especially at high sun. While the contribution to the



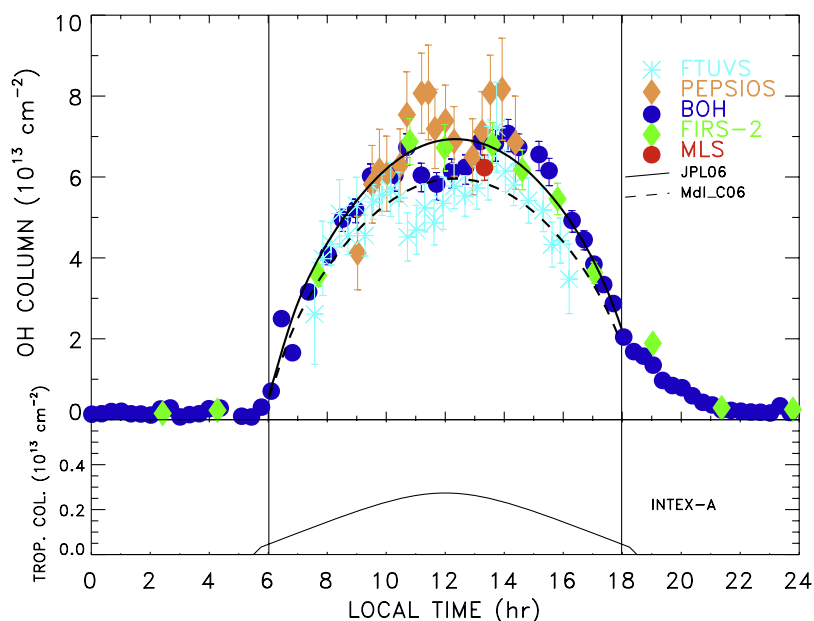


**Figure 15.** Comparison of OH columns for 23 September 2004. (bottom) The total tropospheric correction to the balloon-borne and MLS stratospheric and mesospheric column. (top) These measurements along with the column from two ground-based instruments. Two versions of the model are also shown.

total column from the troposphere is believed to be small (~5%), it should be noted that the FTUVS instrument generally lies above the boundary layer and will therefore receive no contribution to the total column from this region of the atmosphere. The PEPSIOS/FTUVS differences are larger than the expected contribution of boundary layer OH to the total column, and hence unlikely to be the explanation.

[47] As with the balloon-based measurements, the agreement between different column measurement is close, but significant differences between instruments may exist. The column can be a sensitive measure of OH in the stratosphere and mesosphere. Figure 16 shows the fractional contribution to the OH column for different altitude intervals. These fractions were determined from the actual MLS profile for 23 September 2004 above 20 km, modeled OH for 12–21 hPa, and the estimated contributions from the mesosphere and boundary layer. The mesospheric portion (and associated slow chemistry) is responsible for morning-afternoon asymmetries, while the largest contribution comes from the upper stratosphere near the 45 km peak in density. The MLS OH column for this day has increased in v2.2 by 9% compared to v1.5 because of improvements in the MLS mesospheric OH.

### 3.3. Comparison With MAHRSI

[48] The Middle Atmosphere High-Resolution Spectrograph Investigation (MAHRSI) instrument flew on the Space Shuttle in 1994 [Conway *et al.*, 1999] and 1997 [Conway *et al.*, 2000]. We focus on the more recent flight because the observations were made at lower solar zenith angles (SZA) where the OH concentration is higher. We compare the MAHRSI data for 15 August 1997 with a zonal average of MLS data for 7 September 2005 over latitude range of 12–32°S and 33–53°N. This latitude range for the MLS zonal average was selected so that the SZA matched the MAHRSI range (32–49°). The compar-

ison is shown in Figure 17. The MAHRSI points are median values for a given altitude range. The error bars for MLS and MAHRSI OH include precision and systematic errors (2- $\sigma$  root sum of squares). The 2- $\sigma$  uncertainties nearly overlap, but there are correlations in height. A 10 km boxcar average would not overlap nearly as well. It is probabilistically unlikely that the two observations truly agree. At the 42 km OH peak the MAHRSI value is 50% higher than MLS, and at the 70 km OH peak the MAHRSI values are 20% lower than MLS. Below 50 km, the MAHRSI measurements are challenging because of absorption of the OH signal by O<sub>3</sub> at 300 nm wavelength. This systematic error is reflected in the uncertainties.

[49] Figure 17 also shows the results of three model simulations: JPL02, JPL06, and Mdl\_C06. The models were constrained to MLS observations of H<sub>2</sub>O, O<sub>3</sub>, N<sub>2</sub>O, CO, and

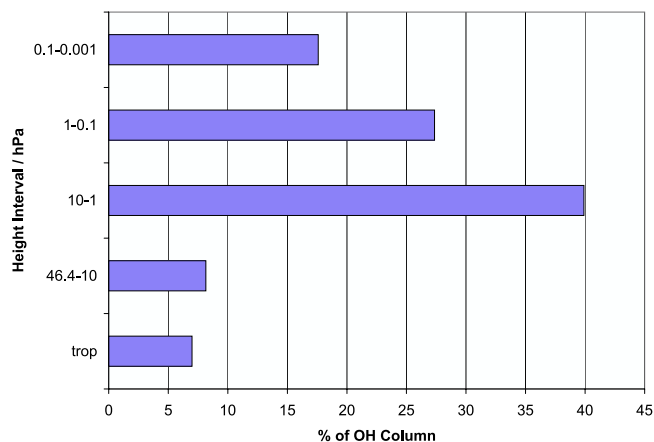


**Figure 16.** Contribution of different height intervals to the total OH column.

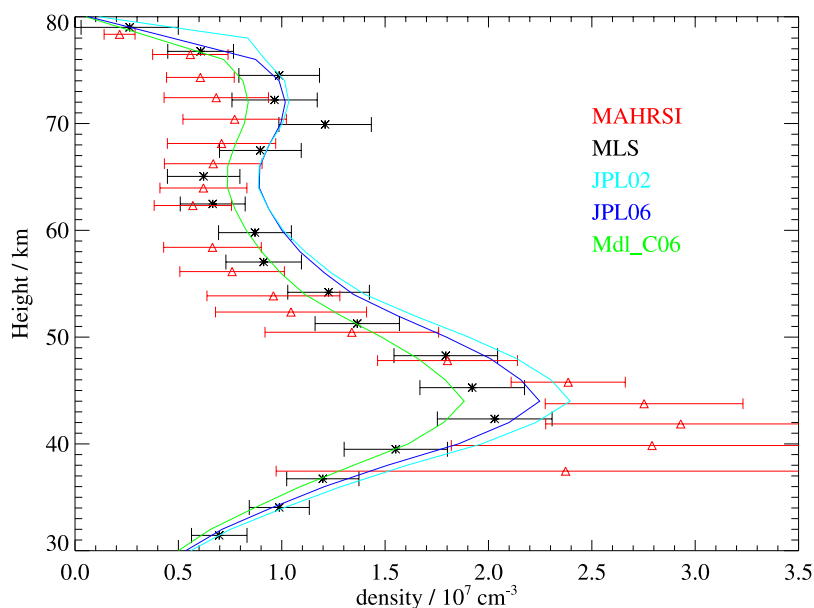


**Figure 17.** MLS OH altitude profiles compared with MAHRSI. The black line with error bars is a zonal average of OH profiles from MLS for 7 September 2005. The MAHRSI median data for 15 August 1997 is denoted by red triangles. The error bars for MLS and MAHRSI OH include precision and systematic errors ( $2\text{-}\sigma$ ). The latitude range ( $12\text{--}32^\circ\text{S}$ ,  $33\text{--}53^\circ\text{N}$ ) for the MLS zonal average was chosen so that the SZA range matches the MAHRSI SZA range ( $32\text{--}49^\circ$ ). Model results for JPL02 (blue line), JPL06 (black line) and Model C06 (green line) are also shown.

temperature that were averaged over the same latitude range as was used for the MLS OH observations. The JPL06 photochemical model using standard chemistry (i.e., recommended rate constants) is in good agreement with MLS over 30–80 km except that MLS has a more pronounced minimum at 63 km. The simulation using JPL06 kinetics results in slightly lower abundances of OH than the JPL02 simulation because of changes to the rate constants for  $\text{O}(^1\text{D})$  quenching and the new recommendation for temperature dependencies of  $\text{O}(^1\text{D}) + \text{H}_2\text{O}$ . Results are also shown for Mdl\_C06 (defined above), which follows from the work of *Canty et al.* [2006] (this earlier paper was based on version 1.5 MLS data and was completed before the JPL06 recommendation was released). Similar to *Canty et al.* [2006], we find the perturbations to the rate constants for  $\text{O} + \text{OH}$  and  $\text{OH} + \text{HO}_2$  that constitute Mdl\_C06 result in overall excellent agreement between measured and modeled OH and HO<sub>2</sub> at all altitudes (Figure 14) and a model profile for OH that falls within the MLS measurement uncertainty at all altitudes.

[50] The shape of the MLS version 2.2 OH profile is simulated well using standard chemistry. This conclusion is consistent with statements by *Pickett et al.* [2006a] and *Canty et al.* [2006], based on version 1.5 MLS data, that the MLS measurements of OH and HO<sub>2</sub> are not consistent with the so-called “HOx dilemma” that resulted from analysis of the MAHRSI observations [*Conway et al.*, 2000; *Summers et al.*, 1997]. We consider it unlikely that changes in H<sub>2</sub>O and O<sub>3</sub> between 15 August 1997 and the time of the MLS observations can account for the different shapes of the OH profile measured by the two instruments. This statement is supported by the fact that *Jucks et al.* [1998] were able to reproduce the model results of *Summers et al.* [1997] using the profiles of H<sub>2</sub>O and OH that were used to interpret the MAHRSI data. Our group has consistently found reasonably good agreement between measured and modeled profiles of OH and we find no evidence for secular changes in H<sub>2</sub>O and OH above 40 km that would be large enough to account for a shift in OH between 1997 and 2005, that is

**Table 3.** Summary of Precisions, Resolution, and Uncertainties for the MLS OH Product

| Region      | Resolution, Vertical $\times$ Horizontal, km | Precision, <sup>a</sup> $10^6 \text{ cm}^{-3}$ | Bias Uncertainty, $10^6 \text{ cm}^{-3}$ | Scaling Uncertainty, % | Comments                      |
|-------------|--|--|--|------------------------|-------------------------------|
| <0.003 hPa  | –  | –  | –  | –                      | unsuitable for scientific use |
| 0.003 hPa   | $5.0 \times 220$                             | 0.6  | 0.034                                    | 90.                    |                               |
| 0.01 hPa    | $2.5 \times 200$                             | 1.3  | 0.031                                    | 41.                    |                               |
| 0.1 hPa     | $2.5 \times 180$                             | 4.2  | 0.12                                     | 3.1                    |                               |
| 1.0 hPa     | $2.5 \times 165$                             | 2.4  | 0.50                                     | 7.                     |                               |
| 10 hPa      | $2.5 \times 165$                             | 8.0  | 0.18                                     | 1.5                    |                               |
| 32–10 hPa   | $2.5 \times 165$                             | 20.0   | 0.50                                     | 1.3                    | use day-night difference      |
| 1000–32 hPa | –  | –  | –  | –                      | unsuitable for scientific use |

<sup>a</sup>Precision on individual profile.

**Table 4.** Summary of Precisions, Resolution, and Uncertainties for the MLS HO<sub>2</sub> Product

| Region      | Resolution, Vertical × Horizontal, km | Precision, <sup>a</sup> 10 <sup>6</sup> cm <sup>-3</sup> | Bias Uncertainty, 10 <sup>6</sup> cm <sup>-3</sup> | Scaling Uncertainty, % | Comments s                    |
|-------------|---------------------------------------|--|--|------------------------|-------------------------------|
| <0.03 hPa   | –                                     | –  | –  | –                      | unsuitable for scientific use |
| 0.046 hPa   | 16 × 600                              | 9.   | 0.39   | 22.                    | use day-night difference      |
| 0.10 hPa    | 16 × 400                              | 16.  | 0.46   | 16.                    | use day-night difference      |
| 1.0 hPa     | 5.5 × 660                             | 18.  | 1.1  | 6.                     | use day-night difference      |
| 10. hPa     | 4.5 × 450                             | 8.   | 37.  | 20.                    | use day-night difference      |
| 1000–21 hPa | –                                     | –  | –  | –                      | unsuitable for scientific use |

<sup>a</sup>Precision on individual profile.

anywhere near the magnitude of the difference between MAHRSI and MLS OH at 40–80 km altitude.

#### 4. Summary and Conclusions

[51] Version v2.2 is a substantial improvement from v1.5 particularly for mesospheric OH and stratospheric HO<sub>2</sub>. Use of v1.5 HO<sub>2</sub> products can benefit from user-applied smoothing, but the internal smoothing in v2.2 is to be preferred because the averaging is done during the retrieval fit. OH in the upper stratosphere is very similar for the two versions.

[52] A summary of the analysis of systematic errors is shown in Table 3 for OH and in Table 4 for HO<sub>2</sub>. For OH, use of day-night differences are recommended for OH at pressures ≥10 hPa because the bias uncertainty becomes zero when the differences are taken. The slope or scaling uncertainty for OH is <8% for pressures >0.003 hPa if due regard is taken of the consistency of THz O<sub>3</sub> measurements as discussed above. Day-night differencing is not needed near 1 hPa because the bias is 0.3% of typical daytime OH densities. In addition, observed night concentrations of OH for 10–0.1 hPa are <1% of noontime tropical values. Use of day-night differences is recommended for HO<sub>2</sub> over the entire usable range of 21–0.03 hPa. The scaling errors for HO<sub>2</sub> are estimated to be larger, as much as 46% at 10 hPa. However, comparison with balloon measurements show that the actual systematic bias for HO<sub>2</sub> at 10 hPa is <20%. Comparisons for both OH and HO<sub>2</sub> balloon measurements, models, and MLS measurements show good agreement, as do the column measurements.

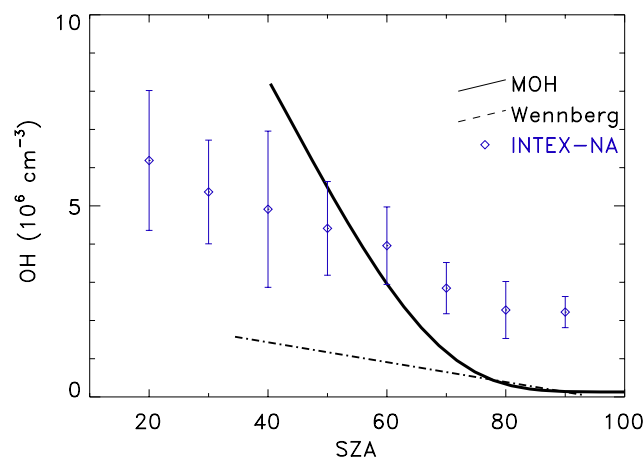
[53] Further work is needed to understand remaining differences among MLS measurements, and balloon instruments, the column measurements of OH, and MAHRSI. In all cases the 2-σ uncertainty nearly overlaps, but there are differences that are unexplained and significant. The results for Mdl\_C06 fall very close to the data, even though the model was not reoptimized for the v2.2 MLS data. The model calculation shows that standard chemistry, with slightly modified rates, is consistent with measured stratospheric and mesospheric MLS HO<sub>x</sub>. This conclusion is consistent with *Canty et al.* [2006], but here we use MLS v2.2 data and kinetics based on JPL 2006 rates. While there are still large uncertainties in the measurements, MLS HO<sub>x</sub> observations do not require new reactions or new rates that differ from recommended values by more than their estimated uncertainties. In this sense, we no longer perceive that there is a “HO<sub>x</sub> dilemma.”

#### Appendix A

[54] The amount of OH in the free troposphere and boundary layer is approximated by the use of aircraft

measurements (Figure A1). Observations of OH taken in the upper troposphere during August 1996 near Hawaii [*Wennberg et al.*, 1998] and the boundary layer region during the INTEX-NA campaign from July to August 2004 in the north eastern US [*Singh et al.*, 2006] are shown. We present here additional boundary layer observations of OH using chemical ionization mass spectrometry taken during 1999–2003 from Meteorological Observatory Hohenpeissenberg (MOH), Germany [*Rohrer and Berresheim*, 2006] to illustrate the variation in measured OH between locations. The polynomial fits to the data taken from Hawaii and Germany are shown (solid and dashed-dotted curves, respectively). The mean and standard deviation of the INTEX-NA data are indicated by blue diamonds and blue lines. The higher values of OH in the boundary layer from the MOH site may be due to ozone rich air during the warm summer, whereas the lower OH values from Hawaii was seen in the colder upper troposphere.

[55] Soundings from the National Weather Service in Albuquerque, NM indicate a boundary layer height of no more than 1.5 km. The INTEX-NA OH data are added to the total column assuming this boundary layer height. The *Wennberg et al.* [1998] values of OH are included from the top of the boundary layer to the lowest level of the balloon observations (12 km) (Figure 15, bottom). The use of the MOH measurements, rather than those from INTEX-NA, lead to a very small increase in total column (not shown). If MOH had been the correct values to use, the maximum amount of OH added to the column would be  $3.4 \times 10^{12}$  cm<sup>-3</sup>, a change in tropospheric contribution of less than 1%.

**Figure A1.** Tropospheric OH versus solar zenith angle.

[56] **Acknowledgments.** We wish to thank all who helped make the Aura HO<sub>x</sub> measurements possible. Thanks to the Aura Project for their support throughout the years (before and after Aura launch), in particular M. Schoeberl, A. Douglass (also as cochair of the Aura validation working group), E. Hilsenrath, and J. Joiner. We also acknowledge the support from NASA Headquarters, P. DeCola for MLS and Aura, and M. Kurylo, J. Gleason, B. Doddridge, and H. Maring, especially in relation to the Aura validation activities and campaign planning efforts. We are grateful to the Columbia Scientific Balloon Facility for launch services. Research at the Jet Propulsion Laboratory, California Institute of Technology, is performed under contract with NASA.

## References

- Blake, G. A., J. Farhoomand, and H. M. Pickett (1986), The far-infrared rotational spectrum of X<sup>2</sup>I OH, *J. Mol. Spectrosc.*, *115*, 226–228.
- Cageao, R. P., J. F. Blavier, J. P. McGuire, Y. B. Jiang, V. Nemtchinov, F. P. Mills, and S. P. Sander (2001), High-resolution Fourier-transform ultraviolet-visible spectrometer for the measurement of atmospheric trace species: Application to OH Source, *Appl. Opt.*, *40*, 2024–2030.
- Canty, T., H. M. Pickett, R. J. Salawitch, K. W. Jucks, W. A. Traub, and J. W. Waters (2006), Stratospheric and mesospheric HO<sub>x</sub>: Results from Aura MLS and FIRS-2, *Geophys. Res. Lett.*, *33*, L12802, doi:10.1029/2006GL025964.
- Conway, R. R., et al. (1999), Middle atmosphere high resolution spectrograph investigation, *J. Geophys. Res.*, *104*, 16,327–16,348.
- Conway, R. R., et al. (2000), Satellite observations of upper stratospheric and mesospheric OH: The HO<sub>x</sub> dilemma, *Geophys. Res. Lett.*, *27*, 2613–2616.
- Froidevaux, L., et al. (2006), Early validation analyses of atmospheric profiles from EOS MLS on the Aura satellite, *IEEE Trans. Geosci. Remote Sens.*, *44*, 1106–1121.
- Froidevaux, L., et al. (2008), Validation of Aura Microwave Limb Sounder stratospheric ozone measurements, *J. Geophys. Res.*, *113*, D15S20, doi:10.1029/2007JD008771.
- Jucks, K. W., et al. (1998), Observations of OH, HO<sub>2</sub>, H<sub>2</sub>O, and O<sub>3</sub> in the upper stratosphere: implications for HO<sub>x</sub> photochemistry, *Geophys. Res. Lett.*, *25*(21), 3935–3938.
- Livesey, N. J., W. V. Snyder, W. G. Read, and P. A. Wagner (2006), Retrieval algorithms for the EOS Microwave Limb Sounder (MLS) instrument, *IEEE Trans. Geosci. Remote Sens.*, *44*, 1144–1155.
- Minschwaner, K., T. Canty, and C. R. Burnett (2003), Hydroxyl column abundance measurements: PEPSIOS instrumentation at the Fritz Peak Observatory and data analysis techniques, *J. Atmos. Sol. Terr. Phys.*, *65*, 335–344.
- Mueller, E. R., et al. (2007), Terahertz local oscillator for the Microwave Limb sounder on the Aura Satellite, *Appl. Opt.*, *46*, 4907–4915.
- Osterman, G. B., et al. (1997), Balloon-borne measurements of stratospheric radicals and their precursors: Implications for the production and Loss of ozone, *Geophys. Res. Lett.*, *24*, 1107–1110.
- Pickett, H. M. (2006), Microwave Limb Sounder THz module on Aura, *IEEE Trans. Geosci. Remote Sens.*, *44*, 1122–1130.
- Pickett, H. M., et al. (2006a), Validation of Aura MLS HO<sub>x</sub> measurements with remote-sensing balloon instruments, *Geophys. Res. Lett.*, *33*, L01808, doi:10.1029/2005GL024048.
- Pickett, H. M., W. G. Read, K. K. Lee, and Y. L. Yung (2006b), Observation of night OH in the mesosphere, *Geophys. Res. Lett.*, *33*, L19808, doi:10.1029/2006GL026910.
- Read, W. G., et al. (2007), Aura Microwave Limb Sounder upper tropospheric and lower stratospheric H<sub>2</sub>O and relative humidity with respect to ice validation, *J. Geophys. Res.*, *112*, D24S35, doi:10.1029/2007JD008752.
- Rohrer, R., and H. Berresheim (2006), Strong correlation between levels of tropospheric hydroxyls and solar ultraviolet radiation, *Nature*, *442*, 184–187.
- Salawitch, R. J., D. K. Weisenstein, L. J. Kovalenko, C. E. Sioris, P. O. Wennberg, K. Chance, M. K. W. Ko, and C. A. McLinden (2005), Sensitivity of ozone to bromine in the lower stratosphere, *Geophys. Res. Lett.*, *32*, L05811, doi:10.1029/2004GL021504.
- Sander, S. P., et al. (2003), Chemical kinetics and photochemical data for use in atmospheric studies, evaluation 14, *JPL Publ.*, 02-25, Jet Propul. Lab., Pasadena, Calif.
- Sander, S. P., et al. (2006), Chemical kinetics and photochemical data for use in atmospheric studies, evaluation 15, *JPL Publ.*, 06-2, Jet Propul. Lab., Pasadena, Calif.
- Singh, H. B., et al. (2006), Overview of the summer 2004 Intercontinental Chemical Transport Experiment–North America (INTEX-A), *J. Geophys. Res.*, *111*, D24S01, doi:10.1029/2006JD007905.
- Smith, I. W. M., and D. W. A. Stewart (1994), Low temperature kinetics of reactions between neutral free radicals, rate constants for the reactions of OH radicals with N atoms (103 ≤ T/K ≤ 294) and with O atoms (158 ≤ T/K ≤ 294), *J. Chem. Soc. Faraday Trans.*, *90*, 3221–3227.
- Stachnik, R. A., J. C. Hardy, J. A. Tarsala, J. W. Waters, and N. R. Erickson (1992), Submillimeter wave heterodyne measurements of stratospheric ClO, HCl, O<sub>3</sub>, and HO<sub>2</sub>: First results, *Geophys. Res. Lett.*, *19*, 1931–1934.
- Summers, M. E., et al. (1997), Implications of satellite OH observations for middle atmospheric H<sub>2</sub>O and ozone, *Science*, *277*, 1967–1970.
- Waters, J. W., et al. (2006), The Earth Observing System Microwave Limb Sounder (EOS MLS) on the Aura satellite, *IEEE Trans. Geosci. Remote Sens.*, *44*, 1075–1092.
- Wennberg, P. O., et al. (1998), Hydrogen radicals, nitrogen radicals, and the production of O<sub>3</sub> in the upper troposphere, *Science*, *279*, 49–53.

T. Canty, B. J. Drouin, R. A. Fuller, N. J. Livesey, V. S. Perun, H. M. Pickett, R. J. Salawitch, S. P. Sander, R. A. Stachnik, W. A. Traub, and J. W. Waters, Jet Propulsion Laboratory, California Institute of Technology, 4800 Oak Grove Drive, Pasadena, CA 91109, USA. (herbert.m.pickett@jpl.nasa.gov)

K. W. Jucks, Harvard-Smithsonian Center for Astrophysics, 60 Garden St., Cambridge, MA 02138, USA.

K. Minschwaner, New Mexico Institute of Mining and Technology, Socorro, NM 87801, USA.